

# GausSurf: Geometry-Guided 3D Gaussian Splatting for Surface Reconstruction

Jiepeng Wang<sup>1</sup>, Yuan Liu<sup>2,3</sup>, Peng Wang<sup>1</sup>, Cheng Lin<sup>1</sup>, Junhui Hou<sup>4</sup>, Xin Li<sup>5</sup>,  
Taku Komura<sup>1</sup>, Wenping Wang<sup>5</sup>

<sup>1</sup>The University of Hong Kong, <sup>2</sup>Hong Kong University of Science and Technology,  
<sup>3</sup>Nanyang Technological University, <sup>4</sup>City University of Hong Kong, <sup>5</sup>Texas A&M University

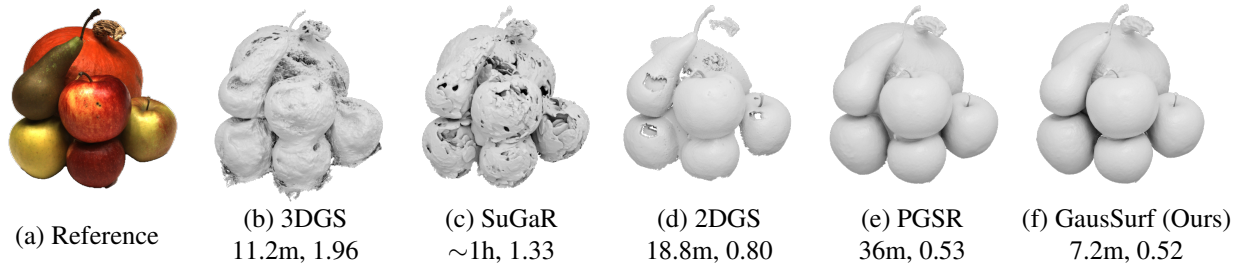


Figure 1. Given a set of posed RGB images (a), our method reconstructs high-quality surfaces (f) with greater efficiency compared to existing Gaussian Splatting-based methods (b-e). In each subcaption (b-f), the first row indicates the reconstruction method, while the second row shows the average reconstruction time and chamfer distance on the DTU dataset, respectively.

## Abstract

3D Gaussian Splatting has achieved impressive performance in novel view synthesis with real-time rendering capabilities. However, reconstructing high-quality surfaces with fine details using 3D Gaussians remains a challenging task. In this work, we introduce GausSurf, a novel approach to high-quality surface reconstruction by employing geometry guidance from multi-view consistency in texture-rich areas and normal priors in texture-less areas of a scene. We observe that a scene can be mainly divided into two primary regions: 1) texture-rich and 2) texture-less areas. To enforce multi-view consistency in texture-rich areas, we enhance the reconstruction quality by incorporating a traditional patch-match based Multi-View Stereo (MVS) approach to guide the geometry optimization in an iterative scheme. This scheme allows for mutual reinforcement between the optimization of Gaussians and patch-match refinement, which significantly improves the reconstruction results and accelerates the training process. Meanwhile, for the texture-less areas, we leverage normal priors from a pre-trained normal estimation model to guide optimization. Extensive experiments on the DTU and Tanks and Temples datasets demonstrate that our method surpasses state-of-the-art methods in terms of reconstruction quality and computation time. Project page: <https://jiepengwang.github.io/GausSurf/>.

## 1. Introduction

Surface reconstruction from multiview images is a long-standing problem in computer graphics and computer vision, which is demanded in downstream tasks such as animation, robotics, and AR/VR. Although intensive works have been done on the multiview surface reconstruction task, fast and accurate surface reconstruction still remains an outstanding problem.

Traditional Multi-View Stereo (MVS) methods [42, 43] are well-established algorithms for multiview surface reconstruction. While MVS methods can achieve high accuracy by pixel-wise matching among different views, they are time-consuming due to their long pipeline including depth estimation, point cloud fusion, surface reconstruction, and texture mapping. Moreover, MVS methods struggle to reconstruct accurate surfaces in areas with low texture due to insufficient features for reliable matching. In recent years, neural rendering methods [44, 45], such as NeuS [47], VolSDF [57] and Neuralangelo [25], provide promising alternatives for multiview surface reconstruction, as these methods enable reconstructing both geometry and appearances in a compact pipeline using a neural shape representation and deliver better reconstruction quality in textureless regions. However, training such neural methods takes extremely long time, typically hours or days, and rendering novel-view images with neural representations is relatively slow.

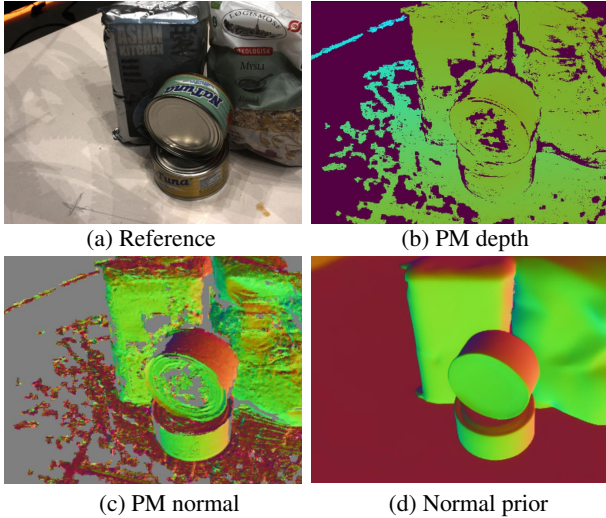


Figure 2. **Visualization of geometric priors.** (Scene 97 in the DTU dataset [1]) (a) Reference image; (b) Refined depth map using patch-match, where the background deep purple color indicates removed unreliable pixels; (c) Refined normal map using patch-match; (d) Estimated normal prior generated by StableNormal [58].

More recently, 3D Gaussian Splatting (GS) [22] has emerged as a promising approach to novel view synthesis due to its real-time rendering capability and efficient training time within several minutes. However, since 3D GS is chiefly designed for novel-view synthesis instead of surface reconstruction, it does not produce high-quality surface reconstruction. SuGaR [15] adapts 3D GS for surface reconstruction by regularizing the Gaussians to be more flattened and produces surfaces with noticeable noisy artifacts. To improve reconstruction quality, 2DGS [16] represents scenes as a set of 2D Gaussian disks and reconstructs high-quality surfaces with surface normal regularizations. PGSR [8] additionally introduces multi-view photometric regularization into the optimization framework of 3D Gaussian Splatting. However, these methods still face challenges, such as relatively limited reconstruction quality or slow optimization speed.

To address these challenges, we propose a new 3D Gaussian Surface-based method, GausSurf, for efficient and high-quality multiview surface reconstruction. We observe that natural scenes typically consist of two types of regions: 1) texture-rich and 2) texture-less. For texture-rich areas, we utilize multi-view consistency constraints to guide the optimization process. For texture-less regions, we incorporate normal priors from a pretrained model to provide supplementary supervision signals. By effectively integrating these geometric priors, our method achieves both high-quality and efficient surface reconstruction.

To improve optimization efficiency and accuracy, we enforce the multiview consistency by iteratively incorporating

stereo matching into the optimization of Gaussians during the training of GausSurf, in addition to rendering losses of supervision by the input images. Specifically, we run the patch-matching algorithm [2] to refine the depth values and normal maps produced by our GausSurf. This enables us to match multiview images to accurately locate the surface positions during the optimization of the Gaussians. Subsequently, the enhanced depth and normal will serve as geometry guidance and supervision signals to further guide the optimization of Gaussians. The Gaussian optimization and patch-match refinement are iteratively conducted to enable mutual reinforcement and lead to robust and efficient surface reconstruction. Note that the traditional MVS also utilizes patch-match for depth and normal refinement, but it conducts surface reconstruction in only one single pass, initialized with coarse depth maps and normal maps from sparse SfM points. These initial depth maps and normal maps usually contain significant errors and noise, leading to degraded MVS reconstruction quality. In contrast, our iterative scheme mitigates this issue by seamlessly integrating the optimization of Gaussians and patch-match refinement, resulting in more robust and efficient reconstruction. During the patch-match process, we also adopt an additional geometric verification strategy, where depth or normal values with discrepancies exceeding a robust threshold across multi-views are considered as unreliable and are discarded. These discarded image regions mean that they don't contain sufficient texture for patch-match and cannot produce reliable depth and normal. Thus, we can classify these pixels as texture-less regions, and incorporate additional normal priors as optimization guidance in these areas.

Extensive experiments demonstrated that our method is capable of reconstructing high-quality surfaces on commonly-used datasets, i.e. the DTU [1] dataset and the Tanks and Temples [23] dataset, and outperforms baseline GS-based surface reconstruction methods in terms of surface quality and reconstruction efficiency. For instance, GausSurf is efficient, costing less than 10 minutes for reconstructing one object with high quality in the DTU dataset.

We summarize our contributions as follows.

- We introduce an efficient framework for high-quality surface reconstruction using 3D Gaussians.
- We integrate the traditional MVS algorithm patch matching and normal priors within our framework to enhance reconstruction fidelity and improve computational efficiency.
- We demonstrate that our method, GausSurf, has superior speed and quality compared to the state-of-the-art GS-based surface reconstruction methods.

We will release the code and data to support future research.

## 2. Related works

In this section, we review works related to multi-view surface reconstruction. Solutions to multi-view reconstruction can be roughly divided into two categories: 1) Multi-view stereo (MVS) methods, which solve for the per-view depth map by maximizing multi-view consistency across views with patch- or feature-level matching and then reconstruct the surface by multi-view fusion; and 2) differentiable rendering-based methods, which maintain a 3D representation for rendering, allowing rendering errors to be back-propagated so the 3D representation can be optimized. The optimized 3D representation can then be post-processed to obtain the final reconstructed surfaces.

### 2.1. Multi-view Stereo

Classical multi-view stereo typically utilizes patch matching across views for each input image to estimate the depth map. Methods like COLMAP [42], OpenMVS [39], and PMVS [14] perform well on texture-rich, plain surfaces but degrade in textureless regions and regions with occlusion boundaries. Learning-based MVS methods, such as MVS-Net [54] and its variants [30, 55, 60, 64], have addressed the degradation problem in textureless regions. However, they still produce unsatisfactory results at occlusion boundaries and lack multi-view consistency due to the manner of depth prediction for each individual view.

### 2.2. Differentiable Rendering

The recent emergence of NeRF [33] and its follow-ups [3–5] has demonstrated the power of differentiable rendering for solving the reconstruction and novel view synthesis tasks. For a detailed review, we refer readers to recent surveys [21, 44, 45].

In this paper, we focus on utilizing differentiable rendering for surface geometry reconstruction.

**Neural fields as representations** A neural field [52] typically represents a function mapping a spatial coordinate to values, which are usually approximated by neural networks [32, 40] or supplemented with feature tables [29, 34, 41]. To represent surface geometry, a neural field typically encodes an implicit function where the surface is defined by a level set. NeRF, though, can inherently encode geometry through volume densities, the surfaces extracted by some isovalue are often of mediocre quality due to the lack of surface constraints. Alternatively, occupancy fields [32] or signed distance fields [40] are more commonly used for surface reconstruction. To supervise the neural field with input images, differentiable surface rendering [27, 35, 37, 56] or differentiable volume rendering [38, 47, 57] are utilized. However, representing those fields by pure neural networks is often inefficient for both training and inference due to the deep network layers.

In addition to representations using pure neural networks, several works have utilized hybrid representations with feature tables, such as voxel grids [6, 24, 51], tri-planes [49], and hash tables [6, 25, 48], to improve training efficiency for fast surface reconstruction. Although these neural reconstruction methods have proven powerful in surface reconstruction, they produce lower-quality rendering results compared to NeRF-like methods due to the addition of regularizations for surface smoothness. Optimizing these neural surface representations is often very time-consuming with more than 12 hours for a single scene.

**Explicit representations** Compared to representations by neural fields, explicit representations such as point clouds [22], voxels [13], and triangle meshes [36, 50] are more interpretable, efficient, and offer better editability. More recently, the explicit representation of 3D Gaussian Splatting [22], which comprises a cloud of semi-transparent 3D Gaussian Primitives, has demonstrated remarkable rendering speed, offering more practicality than neural field-based methods, especially on dynamic scenes [17, 20, 28] and large-scale scenes [10, 26, 53, 63]. Unfortunately, while this point cloud-like representation is beneficial for high-quality rendering, it possesses excessive flexibility, making it challenging to derive a high-quality surface from this representation.

The recent work SuGaR [15] attempts to improve surface reconstruction quality by introducing additional regularizations, encouraging 3D Gaussian primitives to align with a surface. However, its surface extraction method, which involves externally defining a signed distance function based on the Gaussian primitives, fails to accurately represent the ground truth surface, resulting in bubble-like artifacts. NeuSG [9] regularizes the Gaussian primitives to the zero-set of a neural SDF, enabling joint optimization of neural implicit surfaces and 3DGS. However, the reconstruction process is inefficient due to the introduction of neural networks. GSDF [59] and 3DGSR [31] also integrate 3DGS with an extra neural signed distance function. In contrast, our method does not introduce additional neural networks, with better simplicity and efficiency. For other works, 2DGS [16] and Gaussian Surfels [11] utilize 2D Gaussian primitives for better surface alignment, while Gaussian Opacity Fields [62] extract the surface by defining an occupancy field derived from the reconstructed 3DGS. PGSR [8] introduces single-view geometric, multi-view photometric and geometric regularizations in Gaussian Splatting’s framework to improve reconstruction quality. We also incorporate multi-view constraints in the optimization but our strategy is different with PGSR and more efficient. Please refer to the supplementary for more discussions about this point and other related works.

### 3. Method

Given a set of posed images, our goal is to efficiently reconstruct high-quality surfaces from them while achieving photorealistic novel view synthesis at the same time. To achieve this goal, we present a method, called *GausSurf*, that is based on Gaussian Splatting. We regularize 3D Gaussians with multiview stereo (MVS) constraints at texture-rich regions (Sec. 3.2) and normal prior guidance at texture-less areas (Sec. 3.3) to improve reconstruction quality and efficiency. Finally, in Sec. 3.4, we discuss the loss functions and surface extraction process used in GausSurf.

#### 3.1. Preliminary

3D Gaussian Splatting (GS) [22] represents the scene with a set of 3D Gaussians  $\{\mathcal{G}_i\}$ . Each Gaussian is parameterized by an opacity  $\alpha_i$ , its center location  $p_i \in \mathbb{R}^3$  and color  $c_i \in \mathbb{R}^3$ , a rotation  $r_i \in \mathbb{R}^4$  in a quaternion form, and a scale vector  $s_i \in \mathbb{R}^3$ . Thus, the Gaussian distribution in world coordinates is represented by:

$$\mathcal{G}(x) = e^{-\frac{1}{2}(x_i - p_i)^T \Sigma^{-1} (x_i - p_i)} \quad (1)$$

where  $\Sigma = \mathbf{R}(r_i)\mathbf{S}(s_i)\mathbf{S}(s_i)^T\mathbf{R}(r_i)^T$  is the covariance matrix consisting of a scaling matrix  $\mathbf{S}(s_i)$  and a rotation matrix  $\mathbf{R}(r_i)$ .

**Rendering with 3D Gaussians** Given a set of 3D Gaussians, RGB images can be rendered via the splatting procedure [22]. We additionally render normal maps and depth maps from 3D Gaussians. The normal directions are along the axis with the minimum scaling factor. To compute the depth value of a camera ray for a specific Gaussian, we adopt the depth value of the intersection point between the camera ray and the plane with the minimum scaling factor of Gaussians [8].

#### 3.2. Patch-match based Geometry Guidance

Now we explain how to incorporate multiview stereo matching in GausSurf to further improve the reconstruction quality. Specifically, we effectively integrate the patch-match algorithm [2] in optimizing the Gaussian representation. Such a patch-match algorithm enables our method to consider the consistency of neighboring pixels in a patch while pixel-wise rendering only considers the information on a single pixel. Thus, this patch-match algorithm leads to a more accurate surface reconstruction.

To incorporate the MVS constraints, we propose a *refinement and supervision scheme* in an iterative manner. This approach allows GausSurf to leverage the geometry guidance from MVS to optimize Gaussians and concurrently generate more accurate depth and normal maps, which serve as superior initializations for subsequent MVS refinement. Conversely, from the MVS side, an enhanced starting point

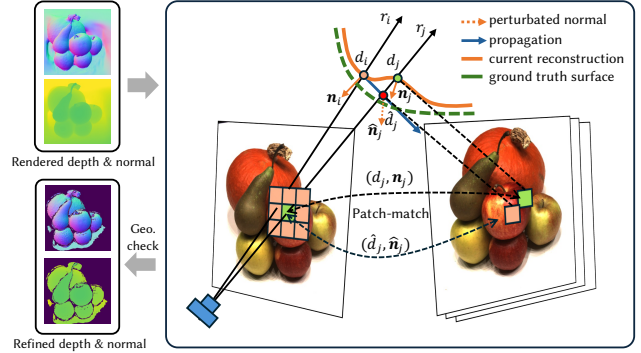


Figure 3. **Patch-match based Geometry Guidance.** Given the rendered depth/normal from Gaussians, we leverage patch-matching to refine the depth and normal for future Gaussian optimization, via propagation, random perturbation and multi-view geometric check.

contributes to more effective and accurate reconstruction and refinement, which also further provides better geometry guidance for the following Gaussian optimization. By employing an iterative scheme, both representations, i.e., Gaussians and MVS refinement, mutually benefit from each other, resulting in robust reconstruction. Specifically, we first initialize the Gaussian representation by training with the rendering losses for a predefined number of steps. Then, we render depth maps and normal maps for all training images and feed the rendered depth maps and normal maps to the patch-match algorithm for refinement. After that, these refined depth maps and normal maps will be used to supervise the Gaussian representation for a specified number of steps along with all other losses. After these optimizing steps, we will render again rendering depth maps and normal maps on all images and repeat this refinement and supervision scheme, which is done iteratively until convergence. In the following, we explain this refinement and supervision scheme in more detail.

**Patch-match for refinement** Given the rendered depth maps and normal maps from Gaussians, we adopt the patch-match idea [2, 43] for refinement. Specifically, for each pixel  $r_i$  of every image, we first propagate the depth value  $d_i$  and normal direction  $\mathbf{n}_i$  of each pixel to its neighboring pixels in a top-to-down and left-to-right order. Then, for each propagated pixel  $r_j$ , we evaluate the patch similarities (NCC)  $s_j$  and  $\hat{s}_j$  with neighboring views on its current depth-normal pair  $(d_j, \mathbf{n}_j)$  and the propagated depth-normal pair  $(\hat{d}_j, \hat{\mathbf{n}}_j)$ , and retain the depth-normal pair with a higher patch similarity. Note that the propagated  $(\hat{d}_j, \hat{\mathbf{n}}_j)$  is augmented with random perturbations before calculating the similarity score. The same propagation-and-patch-match procedure is then repeated again in reverse order over the maps, i.e., bottom-to-up and right-to-left order, to refine

the depth maps and normal maps.

After propagation and patch matching, additional geometric verification is conducted to check the consistency across the depth and normal maps of different images. If the depth or normal differences between different views are larger than a pre-specified threshold, this depth or normal will be regarded as unreliable and removed from the refinement results for this round. The whole patch-match algorithm refines depth maps according to the patch consistency between neighboring views thus greatly improving the depth quality. Due to the propagation scheme, we only need to evaluate NCC on a small number of depth values, contributing to better efficiency.

**Supervision with refined depth** The resulting refined depth maps is then used to supervise the training of the Gaussian representation. Since the geometric verification will discard some unreliable depth values, we only supervise the rendering results from Gaussians at pixels with reliable depth values after geometric verification. The depth prior loss is defined as the L1 loss between MVS depths and rendered depths from Gaussians:

$$\ell_d = \sum |d_p - d_i|, \quad (2)$$

where  $d_p, d_i$  are the patch-match refined depth and rendered depth, respectively.

### 3.3. Normal Prior based Geometry Guidance

Recent advancements in normal estimation have led to significant improvements in reconstruction quality [46, 61]. However, effectively integrating normal priors into GS’s framework remains challenging. We observe that normal priors typically provide high-quality estimations in smooth-surface areas by leveraging evident structural information, yet they tend to produce overly smooth estimations in regions with sharp features. This contrasts with patch-match guidance, which excels in these sharp-feature areas, generating high-quality depth maps. With this observation, we find that normal priors and patch-match refinement can be complementary. Patch-match can be applied effectively in texture-rich areas, while normal priors are more suitable for texture-less regions. This raises the question: how can we accurately distinguish between these two types of regions?

As described in Sec. 3.2, we adopt an additional geometric verification strategy to ensure consistency across the depth and normal maps of different images, where depth or normal values with discrepancies exceeding a robust threshold are considered unreliable and are discarded. We extend this strategy to differentiate pixels in texture-rich and texture-less regions. Pixels passing geometric verification indicate that patch-match can produce accurate depth and normal predictions, and are thus classified as texture-rich. Conversely, pixels failing verification are considered

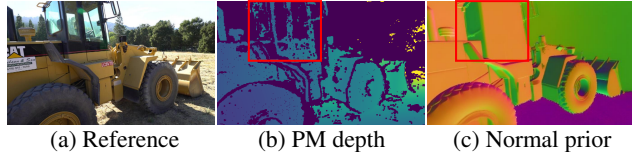


Figure 4. **Visualization of geometric priors.** (Caterpillar in TnT dataset [23]) (a) Reference image; (b) Refined depth map using patch-match, where the background purple color indicates removed unreliable pixels; (c) Estimated normal prior generated by StableNormal [58].

texture-poor, where normal priors are applied as an additional enhancement to achieve high-quality surface reconstruction. Fig. 4 illustrates an example of these distinguished image regions. Through this way, normal priors can be effectively integrated into GausSurf’s framework.

### 3.4. Training Losses and Surface Extraction

Besides the depth loss in patch-match, we also adopt a color rendering loss  $\ell_c$ , a depth-normal consistency loss  $\ell_{nc}$ , and a normal prior loss  $\ell_{np}$ . The color loss is defined as a combination of L1 error of reconstructed images with a D-SSIM term:

$$\ell_c = (1 - \lambda)\mathcal{L}_1 + \lambda\mathcal{L}_{D-SSIM}, \quad (3)$$

where  $\lambda = 0.2$  is used in our experiments. The normal prior loss is used to regularize the rendered normals at texture-less image regions via normal priors:

$$\ell_{np} = \sum (1 - n_p^T n_i), \quad (4)$$

where  $n_p$  is the estimated normal prior from StableNormal[58]. The depth-normal consistency loss [16, 19] enforces the consistency between the normals computed from the rendered depth map and the rendered normal maps by

$$\ell_{nc} = \sum (1 - n_d^T n_i), \quad (5)$$

where  $n_d$  is the normal computed from the rendered depth map while  $n_i$  is the rendered normal map. The total training loss for GausSurf is defined as follows,

$$\ell = \ell_c + \omega_{nc}\ell_{nc} + \omega_{np}\ell_{np} + \omega_d\ell_d \quad (6)$$

where  $\omega_{nc} = 0.5, \omega_{np} = 1.0, \omega_d = 1.0$  are predefined constants.

**Surface extraction** After learning the Gaussian representation, we render depth maps from multiview images and fuse these rendered depth maps with a TSDF-fusion algorithm [18] to obtain the final reconstructed surfaces.

Table 1. **Quantitative comparison on the DTU dataset [1].** We show the Chamfer distance and average optimization time. Our method achieves the highest reconstruction accuracy among other explicit methods. ■, ■, ■ indicate the best, the second best, and the third best respectively.

		24	37	40	55	63	65	69	83	97	105	106	110	114	118	122	Mean	Time
implicit	NeRF [33]	1.90	1.60	1.85	0.58	2.28	1.27	1.47	1.67	2.05	1.07	0.88	2.53	1.06	1.15	0.96	1.49	~ 12h
	VolSDF [57]	1.14	1.26	0.81	0.49	1.25	0.70	0.72	1.29	1.18	0.70	0.66	1.08	0.42	0.61	0.55	0.86	~ 12h
	NeuS [47]	1.00	1.37	0.93	0.43	1.10	<span style="background-color: yellow;">0.65</span>	0.57	1.48	1.09	0.83	0.52	1.20	<span style="background-color: yellow;">0.35</span>	0.49	0.54	0.84	~ 12h
	NeuralWarp [12]	0.49	0.71	0.38	0.38	<span style="background-color: yellow;">0.79</span>	0.81	0.82	1.20	1.06	<span style="background-color: yellow;">0.68</span>	0.66	<span style="background-color: yellow;">0.74</span>	0.41	0.63	0.51	0.68	~ 10h
	Neuralangelo [25]	<span style="background-color: yellow;">0.37</span>	<span style="background-color: yellow;">0.72</span>	<span style="background-color: yellow;">0.35</span>	<span style="background-color: yellow;">0.35</span>	0.87	<span style="background-color: pink;">0.54</span>	<span style="background-color: pink;">0.53</span>	1.29	<span style="background-color: yellow;">0.97</span>	<span style="background-color: yellow;">0.73</span>	<span style="background-color: pink;">0.47</span>	<span style="background-color: yellow;">0.74</span>	<span style="background-color: pink;">0.32</span>	<span style="background-color: pink;">0.41</span>	<span style="background-color: yellow;">0.43</span>	<span style="background-color: yellow;">0.61</span>	~ 12h
explicit	3DGS [22]	2.14	1.53	2.08	1.68	3.49	2.21	1.43	2.07	2.22	1.75	1.79	2.55	1.53	1.52	1.50	1.96	11.2 m
	SuGaR [15]	1.47	1.33	1.13	0.61	2.25	1.71	1.15	1.63	1.62	1.07	0.79	2.45	0.98	0.88	0.79	1.33	~ 1h
	2DGS [16]	0.48	0.91	0.39	0.39	1.01	0.83	0.81	1.36	1.27	0.76	0.70	1.40	0.40	0.76	0.52	0.80	18.8 m
	GOF [62]	0.50	0.82	0.37	0.37	1.12	0.74	0.73	<span style="background-color: yellow;">1.18</span>	1.29	<span style="background-color: yellow;">0.68</span>	0.77	0.90	0.42	0.66	0.49	0.74	2h
	PGSR [8]	<span style="background-color: orange;">0.34</span>	<span style="background-color: orange;">0.58</span>	<span style="background-color: orange;">0.29</span>	<span style="background-color: orange;">0.29</span>	0.78	<span style="background-color: pink;">0.58</span>	<span style="background-color: pink;">0.54</span>	<span style="background-color: pink;">1.01</span>	<span style="background-color: pink;">0.73</span>	<span style="background-color: orange;">0.51</span>	<span style="background-color: orange;">0.49</span>	<span style="background-color: orange;">0.69</span>	<span style="background-color: orange;">0.31</span>	<span style="background-color: orange;">0.37</span>	<span style="background-color: orange;">0.38</span>	<span style="background-color: pink;">0.53</span>	36 m
	Ours	<span style="background-color: orange;">0.35</span>	<span style="background-color: orange;">0.55</span>	<span style="background-color: orange;">0.34</span>	<span style="background-color: orange;">0.34</span>	<span style="background-color: orange;">0.77</span>	<span style="background-color: orange;">0.58</span>	<span style="background-color: orange;">0.51</span>	1.10	<span style="background-color: orange;">0.69</span>	<span style="background-color: orange;">0.60</span>	<span style="background-color: orange;">0.43</span>	<span style="background-color: orange;">0.49</span>	<span style="background-color: orange;">0.32</span>	<span style="background-color: orange;">0.40</span>	<span style="background-color: orange;">0.37</span>	<span style="background-color: orange;">0.52</span>	7.2 m

## 4. Experiments

### 4.1. Implementation Details

All experiments are conducted on a desktop with an i7-13700K CPU and an RTX 3090 GPU. Specifically, for the DTU dataset, we first train the Gaussian model for 2,000 steps to obtain a rough estimate of the geometry before utilizing patch-match refinement. This preliminary model serves as a solid starting point for the subsequent patch-match-based geometry checks. Patch-match refinement is then performed every 1,000 iterations to refine the depth maps and normal maps to provide geometry guidance. This refinement process continues up to 8,000 steps. Following this, we perform another 2,000 iterations to further optimize the Gaussians. This actually leads to 10k optimization steps in total. In the surface extraction with TSDF fusion, we set the voxel size to 0.003 and the truncation threshold to 0.02. Additionally, we utilize the off-the-shelf pretrained method, StableNormal [58], to obtain normal priors, offering supplementary supervision signals.

### 4.2. Evaluation Protocols

**Dataset** We evaluate GausSurf and the baseline methods on the two commonly used datasets, the DTU [1] and the Tanks and Temples [23] dataset. For the DTU dataset, we follow the evaluation protocol of NeuS [47] and 2DGS [16] to evaluate 15 scenes that encompass a wide range of appearances and geometries. We use the original image resolution to run COLMAP to obtain a sparse point cloud for Gaussian initialization and downsample the images to the resolution of  $800 \times 600$  to run our algorithm for both surface reconstruction and novel view synthesis. Additionally, we also test our method on the Tanks and Temples dataset [23] to verify the effectiveness of our method on large-scale scenes. For the NVS task, we test our method on the widely used MipNerf360 dataset [3]. Following 3DGS, we use one image out of every eight images for evaluation and the remaining seven images for training. We report the chamfer distances between the reconstructed surfaces and the

ground-truth surfaces as the metrics for surface reconstruction. We also report the NVS quality in terms of PSNR, LPIPS, and SSIM.

**Baselines** We compare our GausSurf with recent representative multi-view surface reconstruction methods. We categorize them into two groups: 1) neural implicit surface reconstruction methods, such as NeRF [33], NeuS [47], VolSDF [57], NeuralWarp [12] and Neuralangelo [25]; and 2) explicit surface reconstruction methods by Gaussian Splatting, including the vanilla 3D Gaussian Splatting [22], and its follow-up work SuGaR [15]. Additionally, we compare our method with other GS-based works for surface reconstruction, namely 2DGS [16], Gaussian Opacity Field [62], and PGSR [8].

### 4.3. Results

**Surface reconstruction** As shown in Tab. 1, our method achieves the best reconstruction results among all explicit Gaussian-based reconstruction methods. Meanwhile, our method has the lowest reconstruction time among all explicit reconstruction methods with only 7.2 minutes to achieve an accurate reconstruction. The baseline Gaussian-based reconstruction methods commonly take 20 minutes to 1 hour for reconstruction. In GausSurf, the designed patch-match guidance enables accurate estimation of depth values in texture-rich regions and then propagates them to neighboring regions. Meanwhile, the normal priors can also provide additional supervision signals for the texture-less areas. The geometric guidance provide strong guidance to help the Gaussian representation quickly converge to the correct surfaces and reduce the iterations steps. When compared to implicit methods such as NeuS [47] and Neuralangelo [25], our approach achieves competitive reconstruction quality in terms of chamfer distances while requiring significantly less time (7.2 minutes vs. >12 hours). In comparison with NeuralWarp [12] which also adopts patch-match in the reconstruction, our patch-match guidance is much more efficient. With additional propagation, random

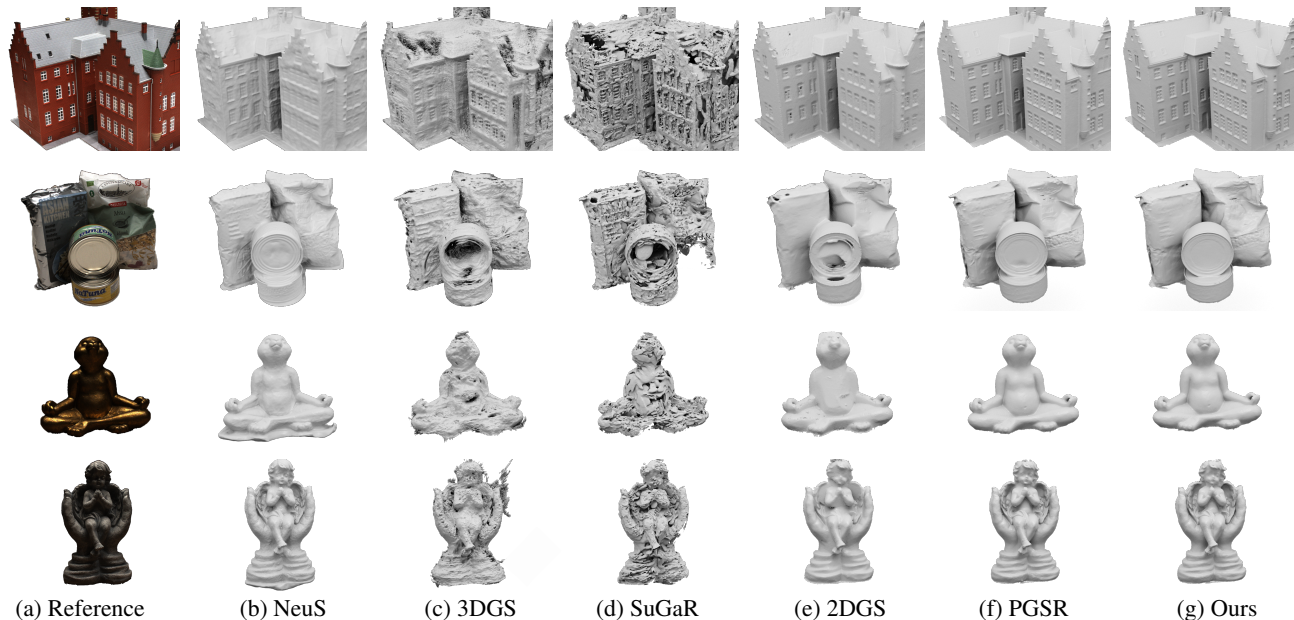


Figure 5. Qualitative comparisons of surface reconstruction on the DTU dataset. Our method can reconstruct more smooth and detailed surface with high efficiency.

Table 2. **Quantitative results of reconstruction results on Tanks and Temples dataset.** Our method achieves comparable reconstruction accuracy (F-score, higher is better) to PGSR with much less optimization time.

	NeuS	Geo-Neus	Neurlangelo	2D GS	GOF	PGSR	Ours
Barn	0.29	0.33	0.70	0.36	0.51	0.66	0.50
Caterpillar	0.29	0.26	0.36	0.23	0.41	0.41	0.42
Courthouse	0.17	0.12	0.28	0.13	0.28	0.21	0.30
Ignatius	0.83	0.72	0.89	0.44	0.68	0.80	0.73
Meetingroom	0.24	0.20	0.32	0.16	0.28	0.29	0.39
Truck	0.45	0.45	0.48	0.26	0.58	0.60	0.65
Mean	0.38	0.35	0.50	0.30	0.46	0.50	0.50
Time	>24h	>24h	>128h	34.2m	2h	1.2h	36.2m

iteration and geometric check strategies for geometry guidance., our model can quickly converge. Fig. 5 presents a qualitative comparison with baseline methods on DTU. Our method can achieve more detailed reconstruction results.

We also quantitatively compare our method with baseline methods on the Tanks and Temples dataset [23], as shown in Table 2. Our method achieves comparable reconstruction performance to the state-of-the-art method PGSR, while requiring much less computation time. Compared to GS-based reconstruction method 2DGS [16], our reconstructed surfaces are much more accurate and smooth with the help of the patch-match and normal prior guidance. Additionally, we also show the qualitative comparisons with these two methods in Fig. 6. Our method can reconstruct more detailed and accurate surfaces.

**Novel view synthesis** Tab. 4 presents the quantitative comparisons of novel view synthesis quality with state-of-the-art GS-based methods, including 3DGS, 2DGS, and

PGSR on the Mip-NeRF360 dataset. Among all baseline methods and our method, GausSurf showcases comparable image fitting quality and generalization abilities to novel poses.

#### 4.4. Ablations

In this section, we ablate the effects of different pipeline modules on reconstruction quality, including the patch-match geometry guidance and normal prior guidance. Table 3 and Fig. 7 show the quantitative and qualitative results of the ablation studies respectively. For the two main modules, we ablate their contributions for reconstruction quality respectively: (a) the patch-match guidance significantly improves the details and accurately locates the correct reconstructed surfaces for GausSurf. (b) the normal prior guidance can further help improve the reconstruction quality. As shown in Table 3, the reconstruction performance primarily originates from the patch-match. On one hand, this demonstrates the effectiveness of our patch-match strategy; on the other hand, we argue that for the DTU dataset, the scenes predominantly contain texture-rich regions, thus are dominated by the patch-match module. We also ablate the effectiveness of the iterative scheme. Please refer to the supplemental for more details.

#### 4.5. Limitations and Future Work

Experiments show that our GausSurf method significantly accelerates the training efficiency compared with existing Gaussian-splatting-based methods, especially in object-level reconstruction scenarios. However, GausSurf still re-

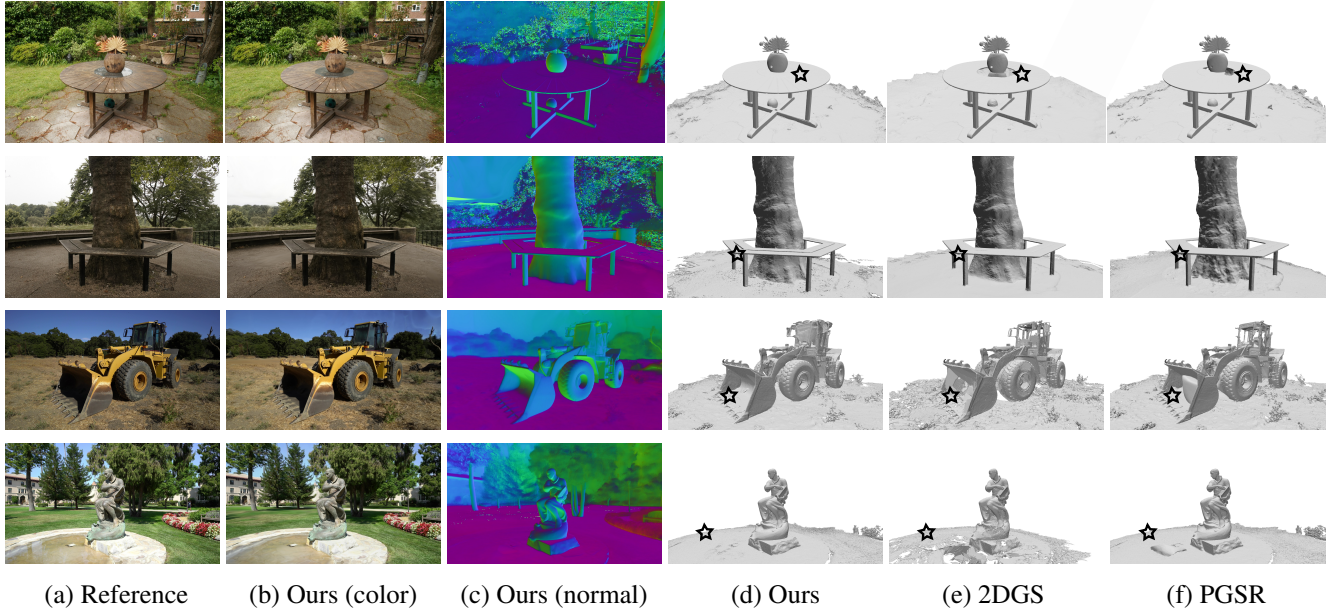


Figure 6. Qualitative comparisons on the MipNerf360 dataset (the first two rows) and TnT dataset (the last two rows). Our method can reconstruct more accurate geometry surface with fine details (See the areas marked with pentagrams).

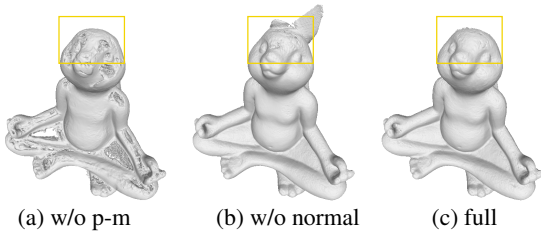


Figure 7. **Ablation study.** Our full setting can achieve the best surface reconstruction results.

Table 3. **Ablation studies of reconstruction quality on the DTU dataset.** We compare the average reconstruction performance on three settings: w/o normal priors, w/o patch-match guidance and our full setting. Our full setting achieves the best performance.

Model setting	w/o normal	w/o p-m	full
CD	0.53	0.93	<b>0.52</b>

quires several minutes per scene optimization, which is not fast enough for real-time applications such as SLAM. In the future, we will explore how to efficiently extend our framework for real-time SLAM reconstruction with streaming video input (e.g., in a feed-forward manner [7]).

We observe that GS-based methods critically rely on various optimization strategies to achieve better quality and efficiency. In this regard, we demonstrate that by combining geometric guidance with 3D Gaussian representation, we are able to efficiently achieve high-quality surface reconstruction. It is noticed that, 2DGS [16] initialize Gaussians directly as 2D disks for surface reconstruction. It would be

Table 4. Quantitative results on the Mip-NeRF360 [4] dataset. All baseline scores are taken directly from the respective papers, when available.

	Outdoor Scene			Indoor scene		
	PSNR $\uparrow$	SSIM $\uparrow$	LIPPS $\downarrow$	PSNR $\uparrow$	SSIM $\uparrow$	LIPPS $\downarrow$
NeRF	21.46	0.458	0.515	26.84	0.790	0.370
Deep Blending	21.54	0.524	0.364	26.40	0.844	0.261
Instant NGP	22.90	0.566	0.371	29.15	0.880	0.216
MERF	23.19	0.616	0.343	27.80	0.855	0.271
BakedSDF	22.47	0.585	0.349	27.06	0.836	0.258
MipNeRF360	24.47	0.691	0.283	31.72	0.917	0.180
Mobile-NeRF	21.95	0.470	0.470	-	-	-
SuGaR	22.93	0.629	0.356	29.43	0.906	0.225
3DGS	<b>24.64</b>	<b>0.731</b>	0.234	30.41	<b>0.920</b>	0.189
2DGS	24.34	0.717	0.246	30.40	0.916	0.195
GOF	24.76	0.742	<b>0.225</b>	<b>30.80</b>	0.928	0.167
PGSR	24.45	0.730	0.224	30.41	<b>0.930</b>	<b>0.161</b>
Ours	<b>25.09</b>	<b>0.753</b>	<b>0.212</b>	30.05	0.920	<b>0.183</b>

interesting to investigate whether appropriate optimization strategies, e.g., iterative patch-match and optimal Gaussian densification strategies could enhance the performance of the 2DGS method. We leave this exploration as future work.

## 5. Conclusion

In this paper, we propose a novel approach for efficient and high-quality surface reconstruction while maintaining the capability of real-time novel view synthesis. We employ incorporating geometric guidance into the framework of 3D Gaussian Splatting. We leverage a patch-match-based Multi-View Stereo (MVS) technique for geometric guidance at texture-rich image areas and normal prior guid-

ance at texture-less image regions to improve reconstruction quality. Extensive experiments demonstrate the effectiveness of our design in surface reconstruction, novel view synthesis and training speed.

## References

- [1] Henrik Aanaes, Rasmus Ramsbøl Jensen, George Vogiatzis, Engin Tola, and Anders Bjarholm Dahl. Large-scale data for multiple-view stereopsis. *International Journal of Computer Vision*, pages 1–16, 2016. [2](#), [4](#)
- [2] Connelly Barnes, Eli Shechtman, Adam Finkelstein, and Dan B Goldman. Patchmatch: A randomized correspondence algorithm for structural image editing. *ACM Trans. Graph.*, 28(3):24, 2009. [2](#), [4](#)
- [3] Jonathan T Barron, Ben Mildenhall, Matthew Tancik, Peter Hedman, Ricardo Martin-Brualla, and Pratul P Srinivasan. Mip-nerf: A multiscale representation for anti-aliasing neural radiance fields. In *Proceedings of the IEEE/CVF International Conference on Computer Vision*, pages 5855–5864, 2021. [3](#), [6](#)
- [4] Jonathan T Barron, Ben Mildenhall, Dor Verbin, Pratul P Srinivasan, and Peter Hedman. Mip-nerf 360: Unbounded anti-aliased neural radiance fields. In *Proceedings of the IEEE/CVF Conference on Computer Vision and Pattern Recognition*, pages 5470–5479, 2022. [8](#)
- [5] Jonathan T Barron, Ben Mildenhall, Dor Verbin, Pratul P Srinivasan, and Peter Hedman. Zip-nerf: Anti-aliased grid-based neural radiance fields. In *Proceedings of the IEEE/CVF International Conference on Computer Vision*, pages 19697–19705, 2023. [3](#)
- [6] Bowen Cai, Jinchu Huang, Rongfei Jia, Chengfei Lv, and Huan Fu. Neuda: Neural deformable anchor for high-fidelity implicit surface reconstruction. In *Proceedings of the IEEE/CVF Conference on Computer Vision and Pattern Recognition*, pages 8476–8485, 2023. [3](#)
- [7] David Charatan, Sizhe Lester Li, Andrea Tagliasacchi, and Vincent Sitzmann. pixelsplat: 3d gaussian splats from image pairs for scalable generalizable 3d reconstruction. In *Proceedings of the IEEE/CVF Conference on Computer Vision and Pattern Recognition*, pages 19457–19467, 2024. [8](#)
- [8] Danpeng Chen, Hai Li, Weicai Ye, Yifan Wang, Weijian Xie, Shangjin Zhai, Nan Wang, Haomin Liu, Hujun Bao, and Guofeng Zhang. Pgsr: Planar-based gaussian splatting for efficient and high-fidelity surface reconstruction. *arXiv preprint arXiv:2406.06521*, 2024. [2](#), [3](#), [4](#), [6](#)
- [9] Hanlin Chen, Chen Li, and Gim Hee Lee. Neusg: Neural implicit surface reconstruction with 3d gaussian splatting guidance. *arXiv preprint arXiv:2312.00846*, 2023. [3](#)
- [10] Kai Cheng, Xiaoxiao Long, Kaizhi Yang, Yao Yao, Wei Yin, Yuexin Ma, Wenping Wang, and Xuejin Chen. Gaussianpro: 3d gaussian splatting with progressive propagation. *arXiv preprint arXiv:2402.14650*, 2024. [3](#)
- [11] Pinxuan Dai, Jiamin Xu, Wenxiang Xie, Xinguo Liu, Huamin Wang, and Weiwei Xu. High-quality surface reconstruction using gaussian surfels. In *SIGGRAPH 2024 Conference Papers*. Association for Computing Machinery, 2024. [3](#)
- [12] François Darmon, Bénédicte Bascle, Jean-Clément Devaux, Pascal Monasse, and Mathieu Aubry. Improving neural implicit surfaces geometry with patch warping. In *Proceedings of the IEEE/CVF Conference on Computer Vision and Pattern Recognition*, pages 6260–6269, 2022. [6](#)
- [13] Sara Fridovich-Keil, Alex Yu, Matthew Tancik, Qinhong Chen, Benjamin Recht, and Angjoo Kanazawa. Plenoxels: Radiance fields without neural networks. In *Proceedings of the IEEE/CVF Conference on Computer Vision and Pattern Recognition*, pages 5501–5510, 2022. [3](#)
- [14] Yasutaka Furukawa and Jean Ponce. Accurate, dense, and robust multiview stereopsis. *IEEE Transactions on Pattern Analysis and Machine Intelligence*, 32(8):1362–1376, 2010. [3](#)
- [15] Antoine Guédon and Vincent Lepetit. Sugar: Surface-aligned gaussian splatting for efficient 3d mesh reconstruction and high-quality mesh rendering. *arXiv preprint arXiv:2311.12775*, 2023. [2](#), [3](#), [6](#)
- [16] Binbin Huang, Zehao Yu, Anpei Chen, Andreas Geiger, and Shenghua Gao. 2d gaussian splatting for geometrically accurate radiance fields. *SIGGRAPH*, 2024. [2](#), [3](#), [5](#), [6](#), [7](#), [8](#)
- [17] Yi-Hua Huang, Yang-Tian Sun, Ziyi Yang, Xiaoyang Lyu, Yan-Pei Cao, and Xiaojuan Qi. Sc-gs: Sparse-controlled gaussian splatting for editable dynamic scenes. *arXiv preprint arXiv:2312.14937*, 2023. [3](#)
- [18] Shahram Izadi, David Kim, Otmar Hilliges, David Molyneaux, Richard Newcombe, Pushmeet Kohli, Jamie Shotton, Steve Hodges, Dustin Freeman, Andrew Davison, et al. Kinectfusion: real-time 3d reconstruction and interaction using a moving depth camera. In *Proceedings of the 24th annual ACM symposium on User interface software and technology*, pages 559–568, 2011. [5](#)
- [19] Yingwenqi Jiang, Jiadong Tu, Yuan Liu, Xifeng Gao, Xiaoxiao Long, Wenping Wang, and Yuexin Ma. Gaussianshader: 3d gaussian splatting with shading functions for reflective surfaces. *arXiv preprint arXiv:2311.17977*, 2023. [5](#)
- [20] Ying Jiang, Chang Yu, Tianyi Xie, Xuan Li, Yutao Feng, Huamin Wang, Minchen Li, Henry Lau, Feng Gao, Yin Yang, et al. Vr-gs: A physical dynamics-aware interactive gaussian splatting system in virtual reality. *arXiv preprint arXiv:2401.16663*, 2024. [3](#)
- [21] Hiroharu Kato, Deniz Beker, Mihai Morariu, Takahiro Ando, Toru Matsuoka, Wadim Kehl, and Adrien Gaidon. Differentiable rendering: A survey. *arXiv preprint arXiv:2006.12057*, 2020. [3](#)
- [22] Bernhard Kerbl, Georgios Kopanas, Thomas Leimkühler, and George Drettakis. 3d gaussian splatting for real-time radiance field rendering. *ACM Transactions on Graphics*, 42(4), 2023. [2](#), [3](#), [4](#), [6](#)
- [23] Arno Knapitsch, Jaesik Park, Qian-Yi Zhou, and Vladlen Koltun. Tanks and temples: Benchmarking large-scale scene reconstruction. *ACM Transactions on Graphics (ToG)*, 36(4):1–13, 2017. [2](#), [5](#), [6](#), [7](#)
- [24] Hai Li, Xingrui Yang, Hongjia Zhai, Yuqian Liu, Hujun Bao, and Guofeng Zhang. Vox-surf: Voxel-based implicit surface representation. *IEEE Transactions on Visualization and Computer Graphics*, 2022. [3](#)

- [25] Zhaoshuo Li, Thomas Müller, Alex Evans, Russell H Taylor, Mathias Unberath, Ming-Yu Liu, and Chen-Hsuan Lin. Neuralangelo: High-fidelity neural surface reconstruction. In *IEEE Conference on Computer Vision and Pattern Recognition (CVPR)*, 2023. 1, 3, 6
- [26] Jiaqi Lin, Zhihao Li, Xiao Tang, Jianzhuang Liu, Shiyong Liu, Jiayue Liu, Yangdi Lu, Xiaofei Wu, Songcen Xu, Youliang Yan, et al. Vastgaussian: Vast 3d gaussians for large scene reconstruction. *arXiv preprint arXiv:2402.17427*, 2024. 3
- [27] Lixiang Lin, Songyou Peng, Qijun Gan, and Jianke Zhu. Fasthuman: Reconstructing high-quality clothed human in minutes. *arXiv preprint arXiv:2211.14485*, 2022. 3
- [28] Youtian Lin, Zuozhuo Dai, Siyu Zhu, and Yao Yao. Gaussian-flow: 4d reconstruction with dynamic 3d gaussian particle. *arXiv preprint arXiv:2312.03431*, 2023. 3
- [29] Lingjie Liu, Jiatao Gu, Kyaw Zaw Lin, Tat-Seng Chua, and Christian Theobalt. Neural sparse voxel fields. *Advances in Neural Information Processing Systems*, 33:15651–15663, 2020. 3
- [30] Keyang Luo, Tao Guan, Lili Ju, Haipeng Huang, and Yawei Luo. P-mvsnet: Learning patch-wise matching confidence aggregation for multi-view stereo. In *Proceedings of the IEEE/CVF International Conference on Computer Vision*, pages 10452–10461, 2019. 3
- [31] Xiaoyang Lyu, Yang-Tian Sun, Yi-Hua Huang, Xiuzhe Wu, Ziyi Yang, Yilun Chen, Jiangmiao Pang, and Xiaojuan Qi. 3dgsr: Implicit surface reconstruction with 3d gaussian splatting. *arXiv preprint arXiv:2404.00409*, 2024. 3
- [32] Lars Mescheder, Michael Oechsle, Michael Niemeyer, Sebastian Nowozin, and Andreas Geiger. Occupancy networks: Learning 3d reconstruction in function space. In *Proceedings of the IEEE/CVF conference on computer vision and pattern recognition*, pages 4460–4470, 2019. 3
- [33] Ben Mildenhall, Pratul P. Srinivasan, Matthew Tancik, Jonathan T. Barron, Ravi Ramamoorthi, and Ren Ng. Nerf: Representing scenes as neural radiance fields for view synthesis. In *ECCV*, 2020. 3, 6
- [34] Thomas Müller, Alex Evans, Christoph Schied, and Alexander Keller. Instant neural graphics primitives with a multi-resolution hash encoding. *ACM transactions on graphics (TOG)*, 41(4):1–15, 2022. 3
- [35] Jacob Munkberg, Jon Hasselgren, Tianchang Shen, Jun Gao, Wenzheng Chen, Alex Evans, Thomas Müller, and Sanja Fidler. Extracting triangular 3d models, materials, and lighting from images. In *Proceedings of the IEEE/CVF Conference on Computer Vision and Pattern Recognition*, pages 8280–8290, 2022. 3
- [36] Baptiste Nicolet, Alec Jacobson, and Wenzel Jakob. Large steps in inverse rendering of geometry. *ACM Transactions on Graphics (TOG)*, 40(6):1–13, 2021. 3
- [37] Michael Niemeyer, Lars Mescheder, Michael Oechsle, and Andreas Geiger. Differentiable volumetric rendering: Learning implicit 3d representations without 3d supervision. In *Proceedings of the IEEE/CVF Conference on Computer Vision and Pattern Recognition*, pages 3504–3515, 2020. 3
- [38] Michael Oechsle, Songyou Peng, and Andreas Geiger. Unisurf: Unifying neural implicit surfaces and radiance fields for multi-view reconstruction. In *Proceedings of the IEEE/CVF International Conference on Computer Vision*, pages 5589–5599, 2021. 3
- [39] openMVS. 3
- [40] Jeong Joon Park, Peter Florence, Julian Straub, Richard Newcombe, and Steven Lovegrove. DeepSDF: Learning continuous signed distance functions for shape representation. In *Proceedings of the IEEE/CVF conference on computer vision and pattern recognition*, pages 165–174, 2019. 3
- [41] Songyou Peng, Michael Niemeyer, Lars Mescheder, Marc Pollefeys, and Andreas Geiger. Convolutional occupancy networks. In *Computer Vision–ECCV 2020: 16th European Conference, Glasgow, UK, August 23–28, 2020, Proceedings, Part III 16*, pages 523–540. Springer, 2020. 3
- [42] Johannes Lutz Schönberger, Enliang Zheng, Marc Pollefeys, and Jan-Michael Frahm. Pixelwise view selection for unstructured multi-view stereo. In *European Conference on Computer Vision (ECCV)*, 2016. 1, 3
- [43] Shuhan Shen. Accurate multiple view 3d reconstruction using patch-based stereo for large-scale scenes. *IEEE transactions on image processing*, 22(5):1901–1914, 2013. 1, 4
- [44] Ayush Tewari, Ohad Fried, Justus Thies, Vincent Sitzmann, Stephen Lombardi, Kalyan Sunkavalli, Ricardo Martin-Brualla, Tomas Simon, Jason Saragih, Matthias Nießner, et al. State of the art on neural rendering. In *Computer Graphics Forum*, pages 701–727. Wiley Online Library, 2020. 1, 3
- [45] Ayush Tewari, Justus Thies, Ben Mildenhall, Pratul Srinivasan, Edgar Tretschk, Wang Yifan, Christoph Lassner, Vincent Sitzmann, Ricardo Martin-Brualla, Stephen Lombardi, et al. Advances in neural rendering. In *Computer Graphics Forum*, pages 703–735. Wiley Online Library, 2022. 1, 3
- [46] Jiepeng Wang, Peng Wang, Xiaoxiao Long, Christian Theobalt, Taku Komura, Lingjie Liu, and Wenping Wang. Neuris: Neural reconstruction of indoor scenes using normal priors. In *European Conference on Computer Vision*, pages 139–155. Springer, 2022. 5
- [47] Peng Wang, Lingjie Liu, Yuan Liu, Christian Theobalt, Taku Komura, and Wenping Wang. Neus: Learning neural implicit surfaces by volume rendering for multi-view reconstruction. *arXiv preprint arXiv:2106.10689*, 2021. 1, 3, 6
- [48] Yiming Wang, Qin Han, Marc Habermann, Kostas Daniilidis, Christian Theobalt, and Lingjie Liu. Neus2: Fast learning of neural implicit surfaces for multi-view reconstruction. In *Proceedings of the IEEE/CVF International Conference on Computer Vision*, pages 3295–3306, 2023. 3
- [49] Yiqun Wang, Ivan Skorokhodov, and Peter Wonka. Pet-neus: Positional encoding tri-planes for neural surfaces. In *Proceedings of the IEEE/CVF Conference on Computer Vision and Pattern Recognition*, pages 12598–12607, 2023. 3
- [50] Markus Worchel, Rodrigo Diaz, Weiwen Hu, Oliver Schreer, Ingo Feldmann, and Peter Eisert. Multi-view mesh reconstruction with neural deferred shading. In *Proceedings of the IEEE/CVF Conference on Computer Vision and Pattern Recognition*, pages 6187–6197, 2022. 3
- [51] Tong Wu, Jiaqi Wang, Xingang Pan, Xudong Xu, Christian Theobalt, Ziwei Liu, and Dahua Lin. Voxurf: Voxel-based

- efficient and accurate neural surface reconstruction. *arXiv preprint arXiv:2208.12697*, 2022. 3
- [52] Yiheng Xie, Towaki Takikawa, Shunsuke Saito, Or Litany, Shiqin Yan, Numair Khan, Federico Tombari, James Tompkin, Vincent Sitzmann, and Srinath Sridhar. Neural fields in visual computing and beyond. In *Computer Graphics Forum*, pages 641–676. Wiley Online Library, 2022. 3
- [53] Yunzhi Yan, Haotong Lin, Chenxu Zhou, Weijie Wang, Haiyang Sun, Kun Zhan, Xianpeng Lang, Xiaowei Zhou, and Sida Peng. Street gaussians for modeling dynamic urban scenes. *arXiv preprint arXiv:2401.01339*, 2024. 3
- [54] Yao Yao, Zixin Luo, Shiwei Li, Tian Fang, and Long Quan. Mvsnet: Depth inference for unstructured multi-view stereo. In *Proceedings of the European conference on computer vision (ECCV)*, pages 767–783, 2018. 3
- [55] Yao Yao, Zixin Luo, Shiwei Li, Tianwei Shen, Tian Fang, and Long Quan. Recurrent mvsnet for high-resolution multi-view stereo depth inference. In *Proceedings of the IEEE/CVF conference on computer vision and pattern recognition*, pages 5525–5534, 2019. 3
- [56] Lior Yariv, Yoni Kasten, Dror Moran, Meirav Galun, Matan Atzmon, Basri Ronen, and Yaron Lipman. Multiview neural surface reconstruction by disentangling geometry and appearance. *Advances in Neural Information Processing Systems*, 33, 2020. 3
- [57] Lior Yariv, Jiatao Gu, Yoni Kasten, and Yaron Lipman. Volume rendering of neural implicit surfaces. In *Thirty-Fifth Conference on Neural Information Processing Systems*, 2021. 1, 3, 6
- [58] Chongjie Ye, Lingteng Qiu, Xiaodong Gu, Qi Zuo, Yushuang Wu, Zilong Dong, Liefeng Bo, Yuliang Xiu, and Xiaoguang Han. Stablenormal: Reducing diffusion variance for stable and sharp normal. *ACM Transactions on Graphics (TOG)*, 2024. 2, 5, 6
- [59] Mulin Yu, Tao Lu, Linning Xu, Lihan Jiang, Yuanbo Xiangli, and Bo Dai. Gsdf: 3dgs meets sdf for improved rendering and reconstruction. *arXiv preprint arXiv:2403.16964*, 2024. 3
- [60] Zehao Yu and Shenghua Gao. Fast-mvsnet: Sparse-to-dense multi-view stereo with learned propagation and gauss-newton refinement. In *Proceedings of the IEEE/CVF conference on computer vision and pattern recognition*, pages 1949–1958, 2020. 3
- [61] Zehao Yu, Songyou Peng, Michael Niemeyer, Torsten Sattler, and Andreas Geiger. Monosdf: Exploring monocular geometric cues for neural implicit surface reconstruction. *Advances in neural information processing systems*, 35:25018–25032, 2022. 5
- [62] Zehao Yu, Torsten Sattler, and Andreas Geiger. Gaussian opacity fields: Efficient high-quality compact surface reconstruction in unbounded scenes. *arXiv:2404.10772*, 2024. 3, 6
- [63] Zhongrui Yu, Haoran Wang, Jinze Yang, Hanzhang Wang, Zeke Xie, Yunfeng Cai, Jiale Cao, Zhong Ji, and Mingming Sun. Sgd: Street view synthesis with gaussian splatting and diffusion prior. *arXiv preprint arXiv:2403.20079*, 2024. 3
- [64] Jingyang Zhang, Shiwei Li, Zixin Luo, Tian Fang, and Yao Yao. Vis-mvsnet: Visibility-aware multi-view stereo network. *International Journal of Computer Vision*, 131(1): 199–214, 2023. 3